JOURNAL OF THERMOPHYSICS AND HEAT TRANSFER
Vol. 10, No. 2, April–June 1996

# Effect of Turbulence on Heat Transfer in Stagnation Flow

H. Al-Salam*
*Fluor Daniel Canada, Inc., Calgary, Alberta T2W 3N2, Canada*
and
A. Haji-Sheikh† and S. M. You‡
*University of Texas at Arlington, Arlington, Texas 76019-0023*

**This article describes an experimental study on the relationship between the heat transfer coefficient $h$ and the standard deviation of velocity of the freestream $u'$ in stagnation flow. The flow is perpendicular to a flat surface with $u'$ measured at the center of the jet between 1.5–3.3 m/s. The data show a linear relationship between $h$ and $u'$. Also, the data compare favorably with heat transfer data in the presence of high freestream turbulence reported by other investigators.**

## Nomenclature

$A$ = exposed heat transfer area, m$^2$
$B_h$ = bias error of $h$
$c_p$ = specific heat W/kg·K
$D$ = diameter of nozzle exit, m
$d$ = diameter of test surface
$h$ = heat transfer coefficient, W/m$^2$·K
$h_0$ = heat transfer coefficient for $u' = 0$, W/m$^2$·K
$Nu$ = Nusselt number
$Pr$ = Prandtl number
$p$ = pressure, kPa
$Re$ = Reynolds number
$r$ = radius of heat transfer surface, m
$St'$ = Stanton number based on $h/\rho c_p u'$
$St'_0$ = Stanton number based on $h_0/\rho c_p u'$
$s$ = sample standard deviation
$T$ = temperature, K
$Tu$ = freestream turbulence, $u'/u_m$
$t$ = time, s
$u'$ = standard deviation of the freestream velocity, m/s
$u_e$ = velocity at exit plane of calibration nozzle, m/s
$u_m$ = mean freestream velocity, m/s
$z$ = axial distance from nozzle exit, m
$\Delta H$ = height, manometer reading in mm of water
$\delta$ = thickness of copper disk
$\theta$ = temperature difference, $T - T_\infty$, K
$\theta_i$ = initial value of $\theta$
$\rho$ = density, kg/m$^3$

*Subscripts*
$a$ = ambient condition
$D$ = length scale as the diameter of nozzle exit
15 = value measured at $y^+ = 15$

## Introduction

STAGNATION flow is encountered in applications such as cooling of high-temperature turbine parts, cooling of electronic components, tempering glass, annealing plastics and metals, drying papers and textiles, and heat treating of metals.

This article investigates heat transfer in stagnation flow in the context of a recent investigation by Maciejewski and Moffat.[1] They reported that there is a linear relationship between the local heat transfer coefficient $h$ and the standard deviation of the local streamwise velocity in the wall-affected region. The theory was verified for turbulent boundary-layer flow in the presence of high and low freestream turbulence. Clearly, stagnation flow is an alternative and a logical system to verify this theory for the following reason: it is relatively easy to produce a stream with freestream turbulence exceeding 20%.

This study investigates the hypothesis that $h$ is also a function of $u'$, for an air jet whose bulk fluid motion is perpendicular to a flat surface. Although this is the first report of this phenomenon, Gardon and Akfirat[2] investigated the effect of turbulence of an air jet on heat transfer from a flat plate. Their results are for the ratio of nozzle-to-plate distance to plate diameter of less than eight nozzle diameters. They also show a correlation between the heat transfer coefficient and the turbulence intensity at the exit plane of the nozzle. Martin[3] presents a review of experimental data on an impinging gas jet to a plate. Hoogendoorn[4] discusses the effect of freestream turbulence on the heat transfer coefficient at the stagnation point of a cylinder in crossflow and reports data for stagnation flow over a flat wall. Jambunathan et al.[5] present a comprehensive literature search on heat transfer for a single circular jet impinging on a flat plate. Finally, Lytle and Webb[6] studied heat transfer for a nozzle-to-plate spacing of less than one nozzle diameter.

Maciejewski and Moffat[1] hypothesized that for high freestream turbulence, e.g., $Tu > 20\%$, the heat transfer coefficient is related to the standard deviation of freestream velocity. In the absence of freestream turbulence or for low $Tu$, they used the maximum $u'$ located at $y^+ \approx 15$ in a fully established turbulent boundary layer. A viable model to verify the hypothesis is the study of heat transfer in stagnation flow where it is possible to provide a constant $u'$. According to the data presented in Ref. 2, the test model must be located at least 10 nozzle diameters downstream from the nozzle to establish a fully turbulent flow; this will ensure that the core is turbulent.

A nozzle is selected for this study and air is impinged perpendicular to a flat circular disk (Fig. 1). The nozzle satisfies the required conditions: $u'$ is constant over an area exceeding the surface area of the disk and the freestream turbulence intensity exceeds 20%. The coefficient $h$ and the standard deviation $u'$ are obtained experimentally and the average heat transfer coefficient is determined. The existence of a linear relationship between $h$ and $u'$ is studied.

The experimental procedures used in this study are not designed to show radial variations in $h$ from the center of the

Received Feb. 6, 1995; revision received Oct. 13, 1995; accepted for publication Oct. 19, 1995. 

*Process Engineer, 10101 Southport Road, S.W.
†Professor, Department of Mechanical and Aerospace Engineering. Senior Member AIAA.
‡Assistant Professor, Department of Mechanical and Aerospace Engineering.

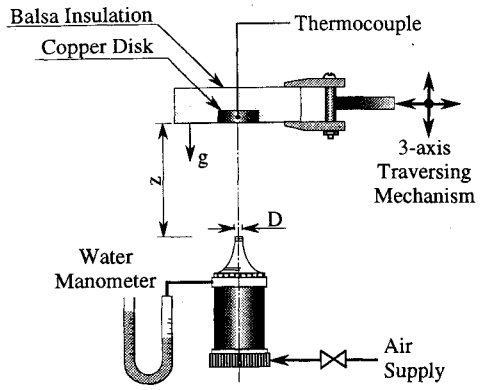


**Fig. 1 Experimental setup for heat transfer measurement.**

jet. However, it is important to prove that the radial variation of $h$ is negligible. To accomplish this task, a second nozzle is used to produce a jet of air with a diameter of about 25% of the diameter of the disk. The objective is to compare results from the two nozzles. A significant reduction in the average heat transfer coefficient using the second nozzle implies that the radial variation of the heat transfer coefficient is detectable. The data reported in this article confirm that the heat transfer coefficient for the primary nozzle is nearly uniform.

## Experimental Setup

The experimental setup employs a transient measurement technique that uses a copper disk. The surface of the copper disk has a diameter of 38 mm and the thickness of the disk is 12.7 mm. One surface of a copper disk serves as a flat plate for heat transfer measurement. The opposite surface and the edges of the copper disk are insulated. Preliminary testing revealed that the insulating materials must have low heat capacity and low thermal conductivity. For this reason, the copper disk was embedded inside a block of balsa wood with one side exposed. The copper disk was heated externally by bringing it in contact with an electrically heated steel cylinder 30 mm in diameter. This ensures that the heat transfer into the balsa wood will be confined to a thin layer. An analytical solution of the temperature field showed that this scheme minimizes the error in the measured heat transfer coefficient. For the range of expected heat transfer coefficient, $h < 200$ W/m$^2\cdot$K, the Biot number $h\delta/k < 0.0075$ indicates a negligible temperature variation within the disk in a direction perpendicular to the surface of the disk. Also, the radial variation of temperature in the copper is small since $hd/k < 0.023$. Accordingly, a lumped-heat-capacitance model is a useful tool for this experimental study. A transient technique yields an average heat transfer coefficient under a spatially constant wall temperature condition.

A 2-mm diameter hole was drilled from the back side of the copper disk toward the centroid of the copper disk. A copper-constantan thermocouple was affixed to the disk with high thermal conductivity epoxy. The calibration of the thermocouple was verified at the ice point and at the boiling point of the water. The assembled copper disk and balsa block were mounted on a platform, and the platform was mounted on a three-axes traversing mechanism (see Fig. 1).

### Nozzles

Two nozzles with markedly different design and flow characteristics are used in this study and the primary nozzle is referred to as Nozzle I. Nozzle I is manufactured by BETE, Inc. (model XA-PR150-B) for combustion and materials processing applications. It accepts air alone or air plus a liquid. The diameter of the nozzle is $D \cong 1$ mm. Under normal operating conditions the pressure drop across this nozzle is sufficiently high to produce near sonic velocity at the nozzle's exit plane.

The secondary nozzle is a research-quality flow nozzle manufactured by DISA (now DANTEC), designed for the calibration of hot-wire anemometers (model 55D45 nozzle package with 55D44 pressure control unit). The diameter of this nozzle, referred to as Nozzle II, is $D = 3.91$ mm. The flow in the nozzle is incompressible and can be approximated as isentropic; however, flow becomes fully turbulent at 10 nozzle diameters downstream.

### Instrumentation

The temperature-measuring device consists of an HP-3852A data acquisition/control unit that includes a voltmeter with better than 1-$\mu$V resolution and a 44708F multiplexer. The temperatures of the copper test model and ambient fluid are measured using 30-gauge copper/constantan thermocouples. This instrument interfaces via IEEE-488 cables to a personal computer that serves as the controller. The calibration of the thermocouple and data acquisition system is checked routinely.

The velocity-measuring instrument is a Dantec three-channel hot-wire anemometer system. However, the bulk of the velocity data was gathered using a single-wire, 5-$\mu$m probe. The velocities were measured without the test model in the plane of impingement at $z/D$ equal to that for the plate during the heat transfer test. This provides the most relevant information for studying the stagnation flow and comparing the results with the data reported in the literature. This scheme is routinely used by other investigators (see Ref. 4, p. 1336 and Ref. 10, p. 1235). The probe was mounted on the traversing mechanism, instead of the copper disk shown in Fig. 1, and the axial component of velocity was measured in radial or axial directions in the jet. Before using the constant temperature anemometer (CTA), velocity vs voltage variations at the exit plane of the calibration nozzle were measured and fed to the Dantec software.

## Velocity Characteristics of Nozzles

The velocity from each nozzle is expected to vary radially from the center of the jet and axially in the direction of flow. The variation of the temporal mean of axial velocity, $u_m$ and root mean square of its fluctuating velocity component $u'$ in the radial direction were studied and data are presented in Figs. 2 and 3. Figures 2 and 3 describe the nature of flow and turbulence for the two nozzles. Figure 2 shows that the mean velocity of Nozzle I suffers little change within the first 5 mm along the radial direction and velocity 20 mm from the center of the spray is about 30% less than the maximum velocity at $r = 0$. In contrast, the mean velocity of Nozzle II reduces from about 12 m/s at $r = 0$ to 4 m/s at a distance of only 4 mm (Fig. 3). The value of $u'$ for both nozzles shows little dependence on the radial coordinate, a prerequisite condition for selecting these nozzles. The changes in the value of the tur-

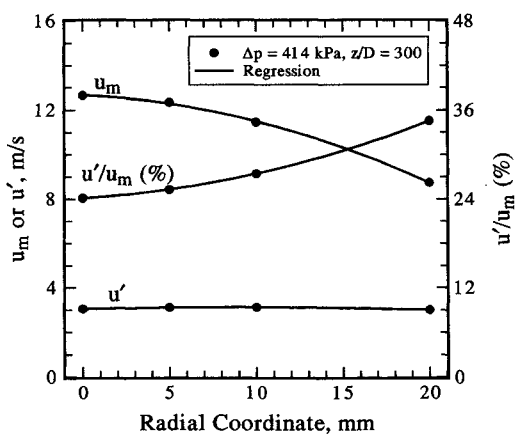


**Fig. 2 Radial variation of $u_m$, $u'$, and turbulence for Nozzle I.**

bulent intensity $u'/u_m$ are attributed to the changes in the values of the mean velocity $u_m$.

The values of $u_m$ and $u'$ at the center of the jet are chosen as reference quantities in subsequent studies. The measurement of $u'$ is repeated five times for each pressure drop and the results are summarized in Table 1 for Nozzle I and Table 2 for Nozzle II. For each test, approximately 8000 samples are taken at a sample rate of 0.5 kHz. This results in sample time intervals of nearly 16 s. Each five-set entry shown in Tables 1 and 2 exhibits consistent results, thereby verifying the accuracy of the sample rate. The variations of $u_m$ and $u'$ for different nozzle inlet gauge pressures are also given in Tables 1 and 2. The velocity measurements for Nozzle I are at two axial distances from the nozzle-exit plane, $z/D$ = 300 and 400. Notice that $u'$ and $u_m$ in Table 1 increase at the same rate as the inlet pressure increases, indicating that the ratio of $u'/u_m$ remains nearly constant. A similar behavior is observed in Table 2 for Nozzle II. However, the ratio $u'/u_m$ slightly increases as the pressure increases. Accordingly, inlet pressures of the nozzles are changed to alter the value of $u'$ and to study the dependence of $h$ on $u'$.

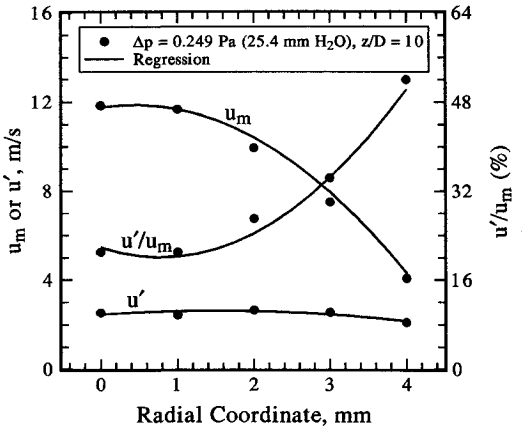


**Fig. 3 Radial variation $u_m$, $u'$, and turbulence for Nozzle II.**

## Heat Transfer Coefficient Measurement

A Hewlett-Packard data acquisition system collects temperature and time data. Fifty data points are collected in 15 s. This procedure is repeated 10 times at the same nozzle inlet pressure, for a range of initial temperatures typically between 80–120°C. Data is collected for different nozzle inlet pressures for both nozzles. Assuming that the heat transfer coefficient and thermophysical properties are constant within a narrow range of temperature, the heat transfer coefficient is related to temperature by the relation

$$h = (mc_p/At)\ell n[\theta_i/\theta(t)] \tag{1}$$

where $t$ is the elapsed time, $\theta(t) = T(t) - T_a$, $\theta_i = \theta(0)$, $m$ is the mass of solid, $c_p$ is the specific heat of solid, and $A$ is the exposed area of the copper disk. When $t$ is small this equation yields $h$ values with large errors. Collecting data over a lengthy time period is avoided because the changes in temperature can adversely affect the thermophysical properties. An uncertainty analysis can identify the time corresponding to acceptably accurate estimates of the heat transfer coefficient within a short time period.

The method first proposed by Kline and McClintock[7] is used here in determining the magnitude of uncertainty associated with the measurements of $h$ for the present experiments. Established guidelines are adopted to categorize the type of experimental error as either bias or precision errors. The bias error is an estimate of the magnitude of the fixed, constant error due to limitation of instrumentation. The precision error is a measure of the repeatability of the data and is expressed in terms of the standard deviation $s$ of the data.

The uncertainty in $h$ due to bias error is dominated by the uncertainty in temperature measurements. The heat transfer model chosen for the present experiments is highly sensitive to the accuracy of the temperature measurements. The bias error of parameter $h$ is $B_h$ and it is defined using Ref. 7 and Eq. (1) as

$$B_h/h = [1/\ell n(\theta_i/\theta)]\sqrt{(B_\theta/\theta)^2 + (B_{\theta_i}/\theta_i)^2} \tag{2}$$

**Table 1 Average centerline velocities $u_m$ and $u'$ for $z/D$ = 300 and 400, and different values of inlet pressure, Nozzle I**

| $z/D$ | 300 | | | | 400 | | | | |
|---|---|---|---|---|---|---|---|---|---|
| $\Delta p$, kPa | 207 | 276 | 345 | 414 | 207 | 276 | 345 | 414 | 483 |
| $u_m$, m/s | 8.20 | 9.89 | 11.20 | 12.63 | 6.03 | 7.26 | 8.25 | 9.10 | 10.13 |
| $u'$, m/s | | | | | | | | | |
| Run 1 | 2.02 | 2.47 | 2.79 | 3.12 | 1.62 | 1.82 | 2.13 | 2.31 | 2.55 |
| Run 2 | 2.04 | 2.47 | 2.78 | 3.11 | 1.50 | 1.82 | 2.11 | 2.39 | 2.52 |
| Run 3 | 2.08 | 2.44 | 2.78 | 3.13 | 1.57 | 1.83 | 2.11 | 2.32 | 2.52 |
| Run 4 | 2.05 | 2.47 | 2.79 | 3.09 | 1.54 | 1.85 | 2.11 | 2.37 | 2.57 |
| Run 5 | 2.01 | 2.44 | 2.78 | 3.05 | 1.53 | 1.84 | 2.12 | 2.37 | 2.51 |
| $u'_{av}$, m/s | 2.04 | 2.46 | 2.78 | 3.10 | 1.55 | 1.83 | 2.12 | 2.35 | 2.53 |
| s, m/s | 0.020 | 0.014 | 0.005 | 0.024 | 0.046 | 0.010 | 0.007 | 0.030 | 0.021 |

**Table 2 Average centerline velocities[a] $u_m$ and $u'$ for $z/D$ = 10 and different values of inlet pressure, Nozzle II**

| $\Delta H$, mm | 10.2 | 15.2 | 20.3 | 25.4 | 30.5 | 35.6 | 40.6 | 45.7 |
|---|---|---|---|---|---|---|---|---|
| $u_m$, m/s | 8.40 | 9.77 | 10.55 | 11.98 | 12.89 | 13.68 | 14.41 | 15.23 |
| $u'$, m/s | | | | | | | | |
| Run 1 | 1.69 | 1.83 | 2.16 | 2.29 | 2.74 | 3.16 | 3.14 | 3.18 |
| Run 2 | 1.77 | 1.87 | 2.13 | 2.43 | 2.74 | 3.05 | 3.10 | 3.32 |
| Run 3 | 1.71 | 1.88 | 2.14 | 2.43 | 2.81 | 3.07 | 3.25 | 3.21 |
| Run 4 | 1.70 | 1.83 | 2.06 | 2.45 | 2.75 | 3.16 | 3.17 | 3.31 |
| Run 5 | 1.71 | 1.87 | 2.17 | 2.29 | 2.84 | 3.08 | 3.14 | 3.33 |
| $u'_{av}$, m/s | 1.72 | 1.86 | 2.13 | 2.38 | 2.78 | 3.10 | 3.16 | 3.27 |
| $s$, m/s | 0.022 | 0.021 | 0.030 | 0.070 | 0.039 | 0.045 | 0.040 | 0.060 |

[a]Nozzle exit velocity is $u_e = 4.05\sqrt{\Delta H}$.

where the bias limits, $B_\theta$ and $B_{\theta_i}$, express the limits of accuracy in the temperature measurements. For the present experiments, the bias limit due to instruments is estimated to be 0.1°C for $\theta$ and $\theta_i$. Figure 4 shows a sample of typical temperature and heat transfer data. The bias error $B_h/h$ is plotted for $\theta_i$ = 20, 40, and 80 K in Fig. 5. Figure 5 shows that the bias errors $B_h/h$ are sensitive to both the relative magnitude of the bias error and to the relative magnitude of temperature. At $\theta_i$ = 80 K the bias (or instrumentation) error on the heat transfer coefficient $B_h/h$ rapidly becomes small for $0.95 < \theta/\theta_i < 0.99$. When $\theta_i$ is reduced to 20 K, the bias error for this range increases to above 8%. For this reason, much of the data reported here are for $\theta_0$ in the vicinity of 80 K. The large scatter in $h$ for relatively small values of time (Fig. 4) reflects the high levels of bias error.

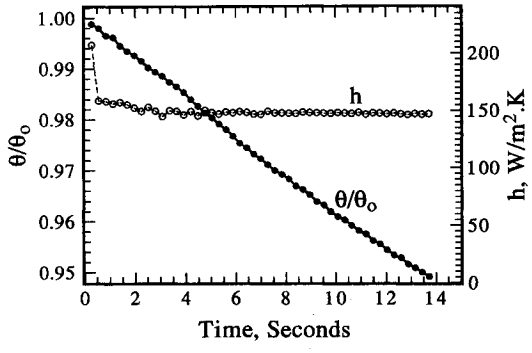


**Fig. 4 Sample temperature and heat transfer data for one run.**

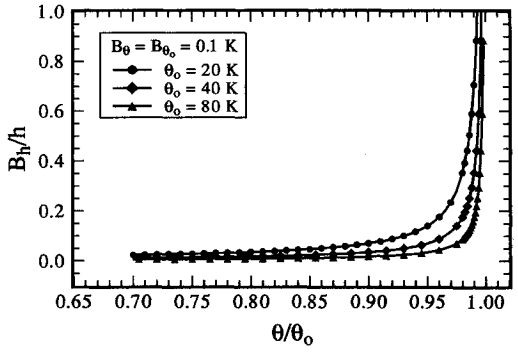


**Fig. 5 Effect of temperature bias error and $\theta_0$ on the bias error of $h$.**

To characterize the precision of the experiments it is necessary to consider the precision within each run and the precision between the repeat runs. Based on the data shown in Fig. 5, the precision within each run is best represented by ignoring the first 10 data points. The large bias error incurred in the initial few data points strongly affects the standard deviation of the data and is not representative of the precision of the experiment. As an example, $h$ is calculated using the data in Fig. 4 and is also plotted in Fig. 4. The standard deviation for all 50 heat transfer coefficient data points is 6% of the mean; however, by ignoring the first 10 data points in Fig. 4 the standard deviation is reduced to 1% of the mean. Accordingly, a measured $h$ reported for a run is an average of the remaining 40 data points. The precision between the repeated runs is determined later. Figure 4 shows that the $\theta$ values change between a narrow range of $0.99\theta_i$ and $0.95\theta_i$; therefore, the mean wall temperature for subsequent computations is $0.97\theta_i$.

The contribution of thermal radiation to the measured heat transfer coefficient data is small. A typical emittance for stably oxidized copper surface is $\varepsilon = 0.5$ (see Ref. 8). The radiation effect reduces the value of $h$ by the quantity $\varepsilon\sigma[(0.97\theta_i + T_a)^4 - T_a^4]/0.97\theta_i$; the surrounding temperature is chosen equal to $T_a$ = 297 K and average wall temperature as $T_w = 0.97\theta_i + T_a$. The estimated correction of radiation effect for the measured $h$ values varies from 4.8 W/m²·K for $\theta_i$ = 100 K and $h >$ 130–3.0 W/m²·K for $\theta_i$ = 0 K and $h >$ 100 W/m²·K; hence, 25% variation in $\varepsilon$ produces an error less than 1% on $h$.

## Results

The measured values of the heat transfer coefficient for Nozzle I at different nozzle inlet pressures are given in Table 3. Each entry is an average of forty values for $h$. The upper portion of the table is for $z/D$ = 300 and the lower portion is for $z/D$ = 400. Ten sets of heat transfer data are given for each combination of $z/D$ values and inlet pressure of the nozzle. Each data set consists of a temperature value $\theta_i$ and $h$. Also, data for Nozzle II, when $z/D$ = 10, are in Table 4. The measured values of the heat transfer coefficient are for eight different inlet pressures and there are 10 temperature and heat transfer values for each inlet pressure.

The main purpose of this study is to establish a relationship between $h$ and $u'$. To establish this relationship for Nozzle I a

**Table 3 Heat transfer coefficient $h$ and temperature $\theta_i$ for $z/D$ = 300 and 400, and different values of inlet pressures, Nozzle I**

| Δp, kPa | 207 | | 276 | | 345 | | 414 | | 483 | |
|---|---|---|---|---|---|---|---|---|---|---|
| z/D | $\theta_i$ | $h$ | $\theta_i$ | $h$ | $\theta_i$ | $h$ | $\theta_i$ | $h$ | $\theta_i$ | $h$ |
| 300 | 66.1 | 113 | 59.0 | 128 | 67.7 | 135 | 47.5 | 133 | — | — |
| | 69.2 | 116 | 66.3 | 124 | 70.4 | 145 | 55.0 | 137 | — | — |
| | 71.4 | 113 | 72.4 | 132 | 71.9 | 147 | 60.7 | 142 | — | — |
| | 75.6 | 113 | 72.7 | 128 | 73.9 | 137 | 65.9 | 142 | — | — |
| | 77.7 | 118 | 74.2 | 130 | 78.2 | 140 | 67.2 | 142 | — | — |
| | 82.8 | 116 | 78.2 | 138 | 82.0 | 146 | 68.2 | 143 | — | — |
| | 84.5 | 119 | 78.5 | 133 | 82.4 | 149 | 75.2 | 143 | — | — |
| | 89.9 | 120 | 80.6 | 139 | 84.4 | 147 | 82.2 | 144 | — | — |
| | 94.8 | 126 | 81.0 | 139 | 88.5 | 149 | 97.3 | 151 | — | — |
| | 97.8 | 129 | 82.7 | 139 | 90.8 | 155 | 108.1 | 159 | — | — |
| 400 | 64.1 | 87 | 78.5 | 112 | 73.2 | 108 | 79.4 | 118 | 50.8 | 116 |
| | 67.8 | 101 | 79.1 | 102 | 82.0 | 117 | 80.6 | 124 | 61.2 | 121 |
| | 68.2 | 97 | 79.4 | 107 | 83.0 | 112 | 83.9 | 115 | 69.1 | 122 |
| | 71.0 | 102 | 79.6 | 105 | 85.1 | 118 | 84.8 | 114 | 77.7 | 123 |
| | 74.1 | 101 | 81.1 | 106 | 85.9 | 116 | 85.8 | 122 | 77.9 | 128 |
| | 82.6 | 100 | 84.8 | 108 | 89.0 | 120 | 87.7 | 132 | 80.5 | 131 |
| | 83.7 | 94 | 87.3 | 103 | 89.3 | 118 | 87.7 | 128 | 81.6 | 141 |
| | 83.9 | 101 | 88.6 | 107 | 92.1 | 116 | 90.2 | 124 | 84.4 | 133 |
| | 84.0 | 96 | 90.2 | 106 | 94.3 | 123 | 91.4 | 123 | 85.9 | 135 |
| | 86.3 | 100 | 91.4 | 115 | 99.2 | 122 | 92.9 | 131 | 87.2 | 135 |

**Table 4 Heat transfer coefficient $h$ and temperature $\theta_i$ for $z/D = 10$ and different values of inlet pressures, Nozzle II**

| $\Delta H$, mm | 10.2 | | 15.2 | | 20.3 | | 25.4 | | 30.5 | | 35.6 | | 40.6 | | 45.7 | |
|---|---|---|---|---|---|---|---|---|---|---|---|---|---|---|---|---|
| Run | $\theta_i$ | $h$ | $\theta_i$ | $h$ | $\theta_i$ | $h$ | $\theta_i$ | $h$ | $\theta_i$ | $h$ | $\theta_i$ | $h$ | $\theta_i$ | $h$ | $\theta_i$ | $h$ |
| 1 | 76.9 | 114 | 70.7 | 116 | 65.2 | 121 | 75.6 | 134 | 75.0 | 141 | 74.6 | 147 | 79.8 | 169 | 71.7 | 159 |
| 2 | 77.0 | 108 | 77.9 | 118 | 71.1 | 125 | 78.6 | 142 | 75.6 | 139 | 75.1 | 146 | 80.1 | 168 | 78.5 | 175 |
| 3 | 77.2 | 132 | 81.0 | 121 | 73.9 | 122 | 81.7 | 146 | 78.2 | 144 | 82.0 | 157 | 80.8 | 170 | 78.7 | 170 |
| 4 | 77.3 | 119 | 81.1 | 123 | 80.7 | 125 | 81.9 | 142 | 81.0 | 148 | 82.1 | 154 | 81.3 | 173 | 80.6 | 169 |
| 5 | 78.6 | 112 | 81.8 | 117 | 83.7 | 133 | 82.7 | 145 | 82.1 | 150 | 84.2 | 157 | 84.0 | 158 | 82.0 | 172 |
| 6 | 79.9 | 117 | 83.2 | 124 | 84.8 | 138 | 83.4 | 144 | 83.0 | 152 | 85.8 | 157 | 89.1 | 172 | 83.6 | 168 |
| 7 | 80.8 | 111 | 86.6 | 126 | 85.5 | 138 | 85.3 | 142 | 84.1 | 151 | 88.2 | 164 | 91.2 | 172 | 84.6 | 174 |
| 8 | 81.1 | 112 | 93.8 | 128 | 90.1 | 141 | 89.2 | 155 | 86.0 | 149 | 88.6 | 164 | 92.9 | 167 | 85.4 | 171 |
| 9 | 87.9 | 114 | 94.9 | 133 | 92.1 | 137 | 89.8 | 149 | 86.2 | 154 | 89.2 | 159 | 94.7 | 166 | 86.4 | 171 |
| 10 | 100.3 | 125 | 95.4 | 128 | 94.1 | 129 | 93.3 | 147 | 94.6 | 158 | 90.3 | 160 | 95.6 | 168 | 87.7 | 174 |

**Table 5 Summary of temperature and velocity data for Nozzle I**

| $z/D$ | $u_m$, m/s | $u'$, m/s | $\theta_0$, K | $h(s, N)$, W/m$^2$·K | $\theta_0$, K | $h(s, N)$, W/m$^2$·K |
|---|---|---|---|---|---|---|
| 300 | 8.20 | 2.04 | 80.1 | 112(1.9, 4) | 81.0 | 114(4.0, 10) |
| | 9.89 | 2.46 | 80.2 | 133(1.8, 4) | 74.6 | 129(4.5, 10) |
| | 11.20 | 2.78 | 80.2 | 139(4.2, 5) | 79.0 | 141(4.5, 10) |
| | 12.63 | 3.10 | 80.7 | 141(2.7, 4) | 72.7 | 139(4.4, 10) |
| 400 | 6.03 | 1.55 | 79.9 | 99(2.6, 6) | 76.6 | 98(3.5, 10) |
| | 7.26 | 1.83 | 80.4 | 106(2.3, 6) | 84.0 | 107(2.8, 10) |
| | 8.25 | 2.12 | 81.8 | 110(3.3, 5) | 87.3 | 112(3.1, 10) |
| | 9.10 | 2.35 | 81.2 | 117(4.6, 6) | 86.4 | 119(4.7, 10) |
| | 10.13 | 2.53 | 80.4 | 127(4.6, 5) | 75.6 | 124(6.3, 10) |

**Table 6 Summary of temperature and velocity data for Nozzle II**

| $u_m$, m/s | $u'$, m/s | $\theta_0$, K | $h(s, N)$, W/m$^2$·K | $\theta_0$, K | $h(s, N)$, W/m$^2$·K |
|---|---|---|---|---|---|
| 8.40 | 1.72 | 80.1 | 109(2.0, 4) | 81.7 | 112(5.4, 10) |
| 9.77 | 1.86 | 80.4 | 115(2.2, 4) | 84.6 | 119(4.3, 10) |
| 10.55 | 2.13 | 80.8 | 125(5.9, 4) | 82.1 | 126(6.4, 10) |
| 11.98 | 2.38 | 80.6 | 138(2.8, 6) | 84.2 | 140(3.7, 10) |
| 12.89 | 2.78 | 80.7 | 143(3.8, 6) | 82.6 | 144(4.4, 10) |
| 13.68 | 3.10 | 79.6 | 147(4.5, 5) | 84.0 | 158(1.4, 10) |
| 14.41 | 3.16 | 80.5 | 166(1.5, 4) | 86.9 | 164(2.9, 10) |
| 15.23 | 3.27 | 80.7 | 166(2.2, 5) | 81.9 | 166(3.0, 10) |

summary of velocity data from Table 1 and heat transfer data from Table 3 are included in Table 5. Columns 5 and 7 in Table 5 contain the heat transfer coefficients $h(s, N)$, where $N$ is the number of data points averaged. The entries in column 5 are average values of 4–6 heat transfer entries from Table 3 and $N$ stands for the number of $\theta_i$ values that are as close as possible to 80 K. The entries in column 7, Table 5, are average values of all 10 repeated data points in Table 3. This strategy improves the precision of the measured data. For a given value of $u_m$ the difference between the entries in columns 5 and 7 in Table 5 is less than 3%. A summary of velocity data for Nozzle II from Table 2 and heat transfer data from Table 4 are included in Table 6.

## Discussion and Remarks

Figure 6 shows the variation of the heat transfer coefficient with $u'$ from Table 5. The data plotted are for mean $\theta_i$ values equal to ≈80 K. Also, Fig. 6 contains data imported from Fig. 3 of Ref. 4 (Nozzles a and b). The turbulence intensity for the imported data is larger than 8%. The data are enveloped between two lines designated by dash lines. The two dash lines are ±9% from the mean value of

$$h = 44 + 35u' \tag{3}$$

shown by a solid line. The data for Nozzle II from Table 6 are also plotted in the same figure. They correlate well with other data within ±9%. The data show no trend to imply a significant change in the average heat transfer coefficient. It is

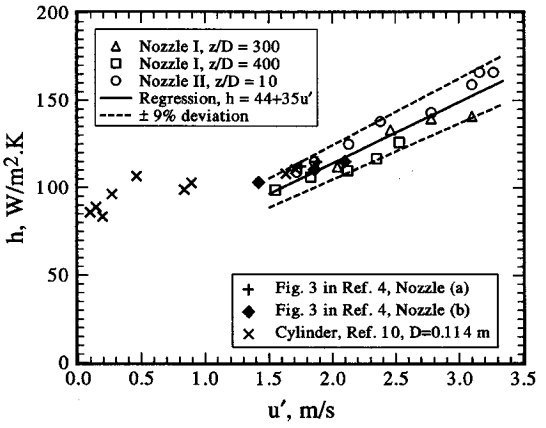


**Fig. 6 Relationship between $h$ and $u'$, when $\theta_0 \cong 80$ K.**

of interest to compare the results with measured stagnation point data for a cylinder in cross flow. Reference 4 shows that the heat transfer data from different investigators vary substantially; Kestin and Wood[9] data are the highest while Lowery and Vachon[10] data are in the midrange. A set of data from Ref. 10 is included in this figure. Note that when $u' \to 0$, $h$ approaches the heat transfer coefficient for laminar flow $h_0$, and when $Tu$ becomes large their data merge with other data. The data of Ref. 9 have much larger values of $h_0$; however, they have low $Tu$ and are not included in Fig. 6.

The data in Fig. 6 clearly agree with the spirit of the theory set forth by Maciejewski and Moffat.[1] Their theory clearly agrees with established boundary-layer theories that the sum of the local values for laminar and turbulent heat flux approximates the wall heat flux; turbulent heat flux dominates when freestream turbulence is high. Note that for stagnation flow, the laminar component of local heat flux dominates until the turbulence is over ~8%; therefore, Eq. (3) approximates the locus of $h$ vs $u'$ values as the turbulence increases.

An examination of heat transfer data in Tables 3 and 4 reveals a slight increase in the heat transfer coefficient as temperature increases. To study this effect, the entries in Table 3 were reproduced for lower values of $\theta_i$ and presented in Table

**Table 7 Heat transfer coefficient $h$ and temperature $\theta_i$ for $z/D$ = 300 and 400, and different values of inlet pressures, Nozzle I**

| $\Delta p$, kPa | 207 | | 276 | | 345 | | 414 | | 483 | |
|---|---|---|---|---|---|---|---|---|---|---|
| $z/D$ | $\theta_i$ | $h$ | $\theta_i$ | $h$ | $\theta_i$ | $h$ | $\theta_i$ | $h$ | $\theta_i$ | $h$ |
| 300 | 18.0 | 112 | 12.9 | 125 | 12.7 | 123 | 18.4 | 139 | — | — |
| | 19.9 | 113 | 13.2 | 131 | 13.2 | 122 | 21.8 | 136 | — | — |
| | 21.9 | 105 | 13.8 | 127 | 13.7 | 138 | 23.1 | 142 | — | — |
| | 24.4 | 110 | 14.7 | 134 | 15.1 | 122 | 27.2 | 143 | — | — |
| | 27.9 | 108 | 15.1 | 124 | 15.4 | 125 | 27.6 | 138 | — | — |
| | 31.7 | 111 | 15.1 | 128 | 15.7 | 128 | 31.2 | 148 | — | — |
| | 35.8 | 114 | 15.5 | 126 | 17.2 | 134 | 35.4 | 147 | — | — |
| | 47.9 | 113 | 17.0 | 128 | 17.8 | 133 | 36.9 | 157 | — | — |
| | 47.9 | 113 | 17.2 | 134 | 21.8 | 135 | 39.9 | 137 | — | — |
| | 54.2 | 118 | 17.6 | 132 | 25.8 | 140 | 45.5 | 137 | — | — |
| 400 | 25.4 | 87.2 | 28.8 | 93.4 | 21.1 | 122 | 24.2 | 109 | 14.3 | 124 |
| | 26.5 | 95.4 | 35.2 | 100 | 23.7 | 116 | 26.9 | 109 | 16.1 | 125 |
| | 27.6 | 92.1 | 35.9 | 99.3 | 25.8 | 110 | 31.1 | 110 | 18.6 | 139 |
| | 28.6 | 92.5 | 39.5 | 96.4 | 28.7 | 110 | 34.5 | 114 | 19.3 | 114 |
| | 30.4 | 89.9 | 39.5 | 102 | 28.8 | 107 | 39.6 | 115 | 21.8 | 114 |
| | 31.2 | 91.7 | 43.4 | 101 | 31.8 | 112 | 44.4 | 115 | 24.3 | 116 |
| | 33.7 | 93.9 | 43.8 | 102 | 32.1 | 106 | 46.2 | 113 | 27.6 | 114 |
| | 34.1 | 94.3 | 48.9 | 104 | 35.0 | 111 | 49.4 | 117 | 28.6 | 129 |
| | 37.3 | 96.5 | 49.0 | 101 | 36.1 | 112 | 56.7 | 117 | 30.9 | 120 |
| | 37.8 | 97.6 | 54.4 | 105 | 40.8 | 114 | 65.9 | 122 | 45.2 | 137 |

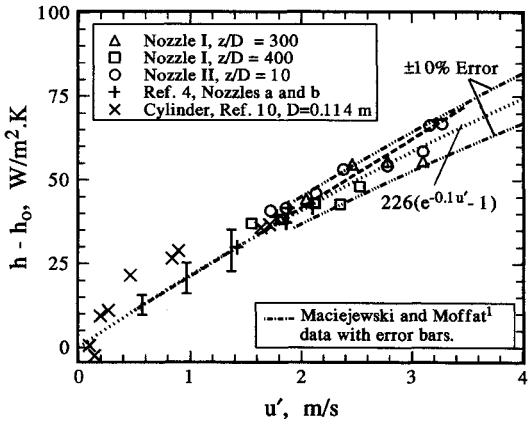


**Fig. 7 Comparison of $h - h_0$ vs $u'$ for stagnation flow data with results from Refs. 1, 4, and 10.**

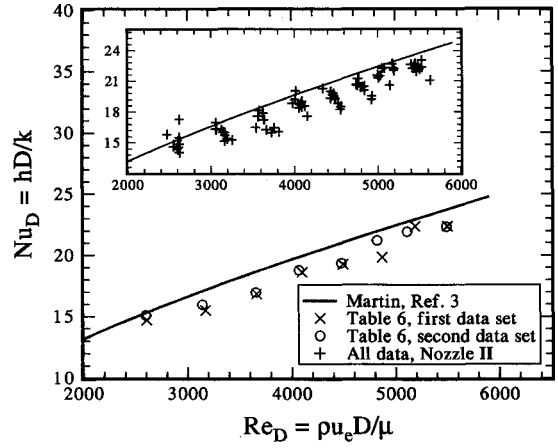


**Fig. 8 Nusselt number as a function of the Reynolds number for Nozzle II and a comparison with the correlation of Martin.[3]**

7. The temperature-dependent thermal conductivity and increase in radiant heat flux are primary contributors to this increase in the heat transfer coefficient as $\theta_i$ increases. To correct data in Tables 3, 4, and 7, they were plotted (not shown) vs $T_w/T_a$. A least-squares curve fitting showed that, for any value of $u'$, $h$ is related to $(T_w/T_a)^n$, where temperature is in degrees Kelvin and $n$ has the average value of $n \cong 0.5$. As discussed earlier, for the range of $\theta_i$ between 0–100 K, approximately 1.8 W/m$^2$·K is the contribution of thermal radiation and the remainder is attributed to the temperature-dependent thermophysical properties. Tables 3 and 7 contain 20 heat transfer data for each set of $u'$ and $z/D$ values. All 20 data are corrected for the temperature effect, averaged, then reduced by a value of $h_0$. To demonstrate the trends of data and for ease of comparison, Fig. 7 contains one entry for each value of $u'$. Figure 7 shows the value of $h - h_0$ plotted vs $u'$, where $h_0$ is a reference heat transfer coefficient representing the average heat transfer coefficient for laminar flow over the test model. The value of $h_0$ is predicted using Eqs. (10–19) in Ref. 11 as

$$h_0 d/k = 0.76\sqrt{2}(u_m d/\nu)^{1/2} Pr^{0.4} \quad (4)$$

To study any radial effect, the process is repeated for Nozzle II, except each of the corresponding data in Fig. 7 is an average of 10 entries from Table 4. The data for Nozzle II agree well with those for Nozzle I and the agreement is better than that observed in Fig. 6. This clearly confirms that there is no detectable spatial variation of the heat transfer coefficient for the primary nozzle, Nozzle I. The dot–dash line in Fig. 7 represents an average value for the data in Fig. 4 of Ref. 1. The dash line in Fig. 7 is a continuation of the dot–dash line. The dash line is an excellent representation of the heat transfer coefficient for stagnation flow when turbulence is high. The plus symbols in the same figure are discrete data points for flow perpendicular to a flat plate, imported from Fig. 3 in Ref. 4. Also, data for a cylinder in crossflow (Ref. 10) are plotted in Fig. 7. The values of $h_0$ for data from Refs. 4 and 10 are calculated as recommended in these references. At small values of $u'$, the heat transfer coefficient for the cylinder shows a rapid increase and it assumes values higher than the dot–dash line. However, as the freestream turbulence increases, the cylinder data join the other data.

The stagnation flow Stanton number $St' = h/\rho c_p u'$ for heat transfer from a flat wall to a jet of air normal to that surface is

$$St' - St'_0 = 0.018 \quad (5)$$

presented in Ref. 1 for high turbulence flow. The subscript 15 refers to a dimensionless distance $y^+ = 15$ where $u'$ was obtained.

According to Ref. 1 and earlier discussion, correlation of experimental heat transfer data for the same Reynolds number while ignoring variation of $u'$ may show large discrepancies. Accordingly, it is of interest to compare the experimental data presented in this article with other published work and to detect any discrepancy. The data for Nozzle II are suitable for such a comparison. The data for Nozzle II and a correlation presented by Martin[3]

$$Nu_D = 2\left(\frac{D}{r}\right)\left[\frac{1 - 1.1D/r}{1 + 0.1(z/D - 6)D/r}\right] Pr^{0.42} Re_D^{0.5} \times \left(1 + \frac{Re_D^{0.55}}{200}\right)^{0.5} \quad (7)$$

are plotted in Fig. 8. This equation is valid for the range of

$$2 \times 10^3 \leq Re_D \leq 4 \times 10^5, \qquad 2.5 \leq r/D \leq 7.5$$

$$2 \leq z/D \leq 12$$

The solid line in Fig. 8 represents Eq. (7). The discrete data points in the main portion of Fig. 8 are taken from Table 6. The discrete data vary slightly, indicating the effect of precision errors. The data in the inset of Fig. 8 are the raw data taken from Table 4. They occupy a wider error band due to both bias and precision errors. The experimental data exhibit the same trend as the solid line, but they are slightly lower. This is not surprising because Nozzle II is part of a precision instrument designed to calibrate hot-wire anemometer probes and, for the same aspect ratios defined in Eq. (7), should produce smoother flow and lower $u'$ than a typical nozzle.

## Conclusions

Researchers studying impinging flow have traditionally put forth the correlation of the Nusselt number in terms of the Reynolds and Prandtl numbers. Often, the persistent discrepancies between results are attributed to the differences in turbulent intensity in the flowfields. The study reported here confirms the assertion by Maciejewski and Moffat[1] that $h$ is a strong linear function of $u'$. This is particularly important because the data from Ref. 1 are for local values of the heat transfer coefficient over a flat plate of a much larger scale. In contrast, the data reported here show that $u'$ directly influences the heat transfer from the wall and this relation is linear for the range of $u'$ studied. The heat transfer coefficient, however, will not increase indefinitely. At higher values of $u'$, the heat transfer coefficient should reach an asymptotic upper limit. This saturation effect was observed at a fixed value of $(u'/u_\infty)\sqrt{Re} \approx 40$ in Refs. 4, 9, and 10. Aside from questions associated with the dependence of this quantity on the size of a test model, it is likely that a saturation of heat flux across the laminar sublayer can occur. An exponential line fitted through the data, dotted line in Fig. 7, is the best fit curve and it exhibits the onset of some saturation effect; however, more data are needed to draw a definitive conclusion. All data are within ±10% of the dotted line, which reduces the deviation of measured $h$ to within ±5%.

## References

[1]Maciejewski, P. K., and Moffat, R. J., "Heat Transfer with Very High Free-Stream Turbulence: Part II—Analysis of Results," *Journal of Heat Transfer*, Vol. 114, No. 4, 1992, pp. 834–839.

[2]Gardon, R., and Akfirat, J. C., "The Role of Turbulence in Determining the Heat Transfer Characteristics of Impinging Jets," *International Journal of Heat and Mass Transfer*, Vol. 8, No. 10, 1965, pp. 1261–1272.

[3]Martin, H., "Heat and Mass Transfer Between Impinging Gas Jets and Solid Surfaces," *Advances in Heat Transfer*, Vol. 13, Academic, New York, 1977, pp. 1–60.

[4]Hoogendoorn, C. J., "The Effect of Turbulence on Heat Transfer at a Stagnation Point," *International Journal of Heat and Mass Transfer*, Vol. 20, No. 12, 1977, pp. 1333–1338.

[5]Jambunathan, K., Lai, E., Moss, M. A., and Button, B. L., "A Review of Heat Transfer Data for Single Circular Jet Impingement," *International Journal of Heat and Fluid Flow*, Vol. 13, No. 2, 1992, pp. 106–115.

[6]Lytle, D., and Webb, B. W., "Air Jet Impingement Heat Transfer at Low Nozzle Plate Spacings," *International Journal of Heat and Mass Transfer*, Vol. 37, No. 12, 1994, pp. 1687–1697.

[7]Kline, S. J., and McClintock, F. A., "Describing Uncertainties in Single-Sample Experiments," *Mechanical Engineering*, Vol. 75, No. 1, 1953, pp. 3–8.

[8]Incropera, F. P., and DeWitt, D. P., *Fundamentals of Heat and Mass Transfer*, Wiley, New York, 1990.

[9]Kestin, J., and Wood, R. T., "The Influence of Turbulence on Mass Transfer from Cylinders," *Journal of Heat Transfer*, Vol. 93, No. 4, 1971, pp. 321–327.

[10]Lowery, G. W., and Vachon, R. I., "The Effect of Turbulence on Heat Transfer from Heated Cylinders," *International Journal of Heat and Mass Transfer*, Vol. 18, No. 11, 1975, pp. 1229–1242.

[11]Kays, W. M., and Crawford, M. E., *Convective Heat and Mass Transfer*, McGraw–Hill, New York, 1993.